

Optomagnetic logic based on optical nonthermal magnetization switching in near-compensated iron-garnets

N.I. Gribova,^{1, 2, 3,*} D.O. Ignatyeva,^{1, 3} N.A. Gusev,¹ A.K. Zvezdin,⁴ and V.I. Belotelov^{1, 3}

¹*Russian Quantum Center, Moscow 121205, Russia*

²*Moscow Institute of Physics and Technology (National Research University), Dolgoprudny 141701, Russia*

³*Lomonosov Moscow State University, Moscow 119991, Russia*

⁴*Prokhorov General Physics Institute of the Russian Academy of Sciences, Moscow 119991, Russia*

(Dated: February 9, 2026)

We propose a set of optomagnetic logic elements based on the effect of optical magnetization switching via the non-thermal inverse Faraday effect induced by femtosecond laser pulses in nearly compensated iron-garnet film with uniaxial anisotropy. Two equilibrium states in such a film are separated by a potential barrier that might be overpassed if the femtosecond pulse fluence exceeds a threshold value, so that magnetization is reversed after the pulse action. The switching threshold depends strongly on the value of applied in-plane external magnetic field, and is different for the two initial magnetization states and two opposite optical pulse helicities. This makes it possible to perform optomagnetic non-thermal deterministic writing of a magnetic bit. Such switching mechanism can be used for realizing reconfigurable optomagnetic logic elements without thermal assistance. Logical operations are implemented by encoding inputs in the amplitude and helicity of the optical pulses, while outputs are written as the magnetization state. The study demonstrates a pathway towards heating-free optomagnetic logic and memory devices.

I. INTRODUCTION

Optical control of magnetization is a cutting-edge problem in spintronics and ultrafast magnetism [1, 2]. Femtosecond laser pulses have been shown to reverse spins at the timescales down to a few picoseconds[3–10], with major implications for high-speed magnetic memory and data processing. The reviews emphasize that photon–magnon interactions in magnets are currently being used to obtain quantum functionalities [11, 12] and control over ultrafast spin dynamics [2, 13]. Experiments span diverse materials: from metallic ferrimagnets to insulating garnets and from rare-earth–transition metal alloys [14] to synthetic multilayers [15]. This broad interest, including proposals for photon–magnon quantum devices [13, 16], underscores the importance of the all-optical switching problem.

So far, all demonstrated optical switching have relied on light absorption, with the switching mechanism being either thermal or non-thermal — the photoinduced magnetic anisotropy. In metallic ferrimagnets (e.g. GdFeCo [17, 18]), the phenomenon of the ultrafast demagnetization caused by electron heating combined by circular dichroism provides all-optical helicity dependent toggle switching without application of any external magnetic field [17–19]. Such kind of switching in metals has a threshold character and substantial laser fluences: e.g. Stanciu et al. [18] reported a threshold around $5.7 \text{ mJ}\cdot\text{cm}^{-2}$; Hennecke et al.[3] showed $5\text{--}6 \text{ mJ}\cdot\text{cm}^{-2}$; Ostler et al.[17] demonstrated switching for energies larger than $2.3 \text{ mJ}\cdot\text{cm}^{-2}$; Vahaplar et al. [19] operated with experimental fluences in the range $2.37\text{--}2.6 \text{ mJ}\cdot\text{cm}^{-2}$.

Though in dielectrics the coupling of light to spins does not rely primarily on the resonant heating of ions; in Co-doped iron garnets (YIG:Co) photo-excitation of localized Co d–d electronic transitions modifies the magnetic anisotropy and enables ultrafast, essentially dissipation-free magnetic switching [5, 20].

On the contrary, in this work we theoretically predict a possibility to switch an optically transparent ferrimagnet purely via the optomagnetic effect, the inverse Faraday effect (IFE) which requires no absorption [21, 22]. The IFE is a manifestation of a Raman-type nonlinear optical process, in which circularly polarized light induces an effective magnetic field acting on the magnetic system. This distinction is crucial for practical implementation of optomagnetic switching in memory and logic devices, as heating reduces the energy efficiency and limits the operating speeds.

We propose to use transparent ferrimagnets in the vicinity of the magnetization compensation point T_m , where the magnetic moments of sublattices are fully compensated. The magnetic phase diagram of ferrimagnets includes the collinear and non-collinear phases, distinguished by the relative orientation of sublattice magnetizations and their alignment with respect to the external magnetic fields [23–26]. The collinear phase is accompanied with collinear alignment of magnetizations of both sublattices and external magnetic field. The non-collinear phase is characterized by bevel of sublattices magnetizations combined with a net magnetization tilted to the external magnetic field. An important feature of the non-collinear phase is an existence of two degenerate equilibrium magnetization states [27]. Spin dynamics of such ferrimagnets is much richer compared to ferromagnetic materials, and includes excitation of the two modes with close frequencies [25], ferromagnetic mode softening and amplitude growth [26] and other peculiar effects

* gribova.ni@phystech.edu

[28–31]. In this work, we reveal a mechanism of optomagnetic nonthermal magnetization switching toggled via IFE, which opens new possibilities for deterministic writing of the magnetic bits and construction of a set of optomagnetic logical elements.

Our study contributes to the fundamental understanding of nonlinear spin dynamics in ferrimagnets and demonstrates the feasibility of nonthermal optomagnetic control of magnetization states. This approach promises energy-efficient spin manipulation, advancing the development of next-generation spintronic and quantum devices with optical control.

II. FERRIMAGNET EQUILIBRIUM STATES AS INFORMATION BITS

Optomagnetic nonthermal switching discussed below can be performed in various ferrimagnets possessing uniaxial anisotropy in the vicinity of their magnetization compensation point and thus enabling of realization of non-collinear phase with the two degenerate magnetization states. As an example of such material, we consider rare-earth iron garnet (RIG). RIG has a formula $R_3Fe_5O_{12}$ with each formula unit containing 3 ions R^{3+} on dodecahedral sites, 2 ions Fe^{3+} on octahedral sites and 3 ions Fe^{3+} on tetrahedral sites [32] and is characterized by a cubic symmetry [33]. RIGs are ferrimagnetic: octahedral and tetrahedral sites Fe^{3+} exhibit antiparallel coupling by exchange interaction, therefore, the uncompensated magnetic moment of antiparallel Fe^{3+} ions results in a net magnetization \mathbf{M}_{Fe} . If the dodecahedral site is magnetic ($R = Gd, Tb$, etc.), R^{3+} couples as nearly anti-parallel to the tetrahedral site of Fe^{3+} with total magnetization \mathbf{M}_R [25]. At the compensation point, the contributions of the magnetic moments of the sublattices balance each other ($\mathbf{M}_R = -\mathbf{M}_{Fe}$), and the resulting magnetization vanishes. The temperature of the magnetic compensation point depends on the type and concentration of rare-earth ions, as well as their magnetic moments and distribution over the sublattices. Additionally, isovalent substitution in the iron sublattices by other elements (e.g., Ga^{3+}, Al^{3+}) can shift the compensation point by altering the balance of magnetic moments [34].

The magnetization state of a RIG film can be described by the Néel vector $\mathbf{L} = \mathbf{M}_{Fe} - \mathbf{M}_R$ and the total magnetization vector $\mathbf{M} = \mathbf{M}_{Fe} + \mathbf{M}_R$ [24, 35, 36], where $\mathbf{M}_i = M_i(\cos \theta_i \cos \phi_i, \cos \theta_i \sin \phi_i, \sin \theta_i)$ with $i = R, Fe$ (Appendix VII). Orientation of $\mathbf{M}_{Fe}, \mathbf{M}_R$ is nearly antiparallel and in static case they both always lie in the plane defined by the external in-plane magnetic field and the anisotropy axis (Fig. 1). Small canting from the antiparallel orientation in non-collinear phase is taken into account in our analysis (Appendix VII), but not discussed further as it has extremely small values $\sim 7 \cdot 10^{-2}$ deg [25], so roughly $\mathbf{L} \parallel \mathbf{M}_R \parallel \mathbf{M}_{Fe}$. The Néel vector is defined in the spherical coordinate system by the angles θ and ϕ . In the further consideration the equilibrium position of \mathbf{L}

is close to the external magnetic field, i.e. to the x -axis. Therefore, it is convenient to use coordinate system as $\mathbf{L} = L(\cos \theta \cos \phi, \cos \theta \sin \phi, \sin \theta)$.

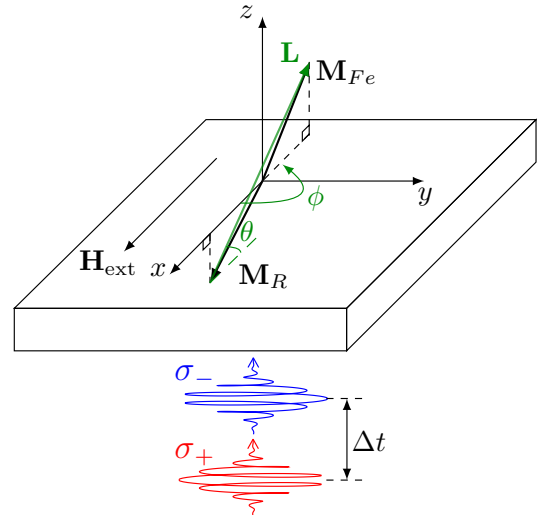


Figure 1: Ferrimagnetic film with uniaxial magnetic anisotropy in the external magnetic field H_{ext} along x axis. The easy axis of the film is along z axis. The θ angle is between \mathbf{L} and XOY plane, ϕ is the angle between the projection \mathbf{L} on the XOY plane and x axis.

The equilibrium states of the two-sublattice system correspond to the minima of the effective potential energy of the system (Fig. 2a), which is obtained using the known relationship between the Lagrangian and the Hamiltonian [25, 28, 37, 38] (Appendix VII) for the stationary case $\dot{\phi} = 0$ and $\dot{\theta} = 0$ [25]:

$$U_{eff} = -\frac{\chi}{2} H_{ext}^2 (\sin^2 \theta \cos^2 \phi + \sin^2 \phi) - m H_{ext} \cos \theta \cos \phi - K \sin^2 \theta, \quad (1)$$

where χ is the transverse magnetic susceptibility defined by the exchange energy, H_{ext} is the external magnetic field, $m = M_{Fe} - M_R$ is the difference between the magnetization moduli of the sublattices, K is the effective magnetic uniaxial anisotropy constant calculated as the sum of sublattice anisotropies K_{Fe} and K_R : $K = K_{Fe} + K_R$. The direction of \mathbf{L} in equilibrium is determined by

$$\cos \theta_0 = \frac{m H_{ext}}{2K + \chi H_{ext}^2}, \quad (2)$$

and $\phi_0 = \pi/2$. Eq. (2) has two solutions, corresponding to two equilibrium states with $+\theta_0$ and $-\theta_0$ (Fig. 2). These states are degenerate, as they have the same potential energy U_{eff} . The height of the barrier between the equilibrium positions is

$$\Delta U_{eff} = -m H_{ext} + \frac{1}{2} [\chi H_{ext}^2 + 2K + \frac{m^2 H_{ext}^2}{\chi H_{ext}^2 + 2K}]. \quad (3)$$

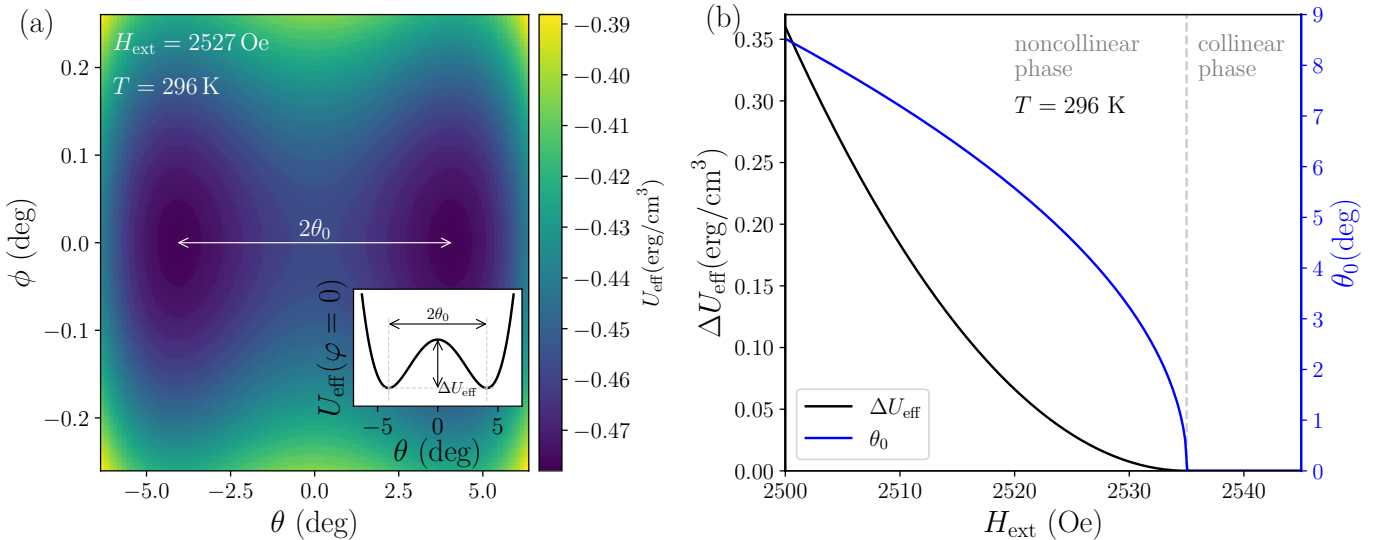


Figure 2: (a): 2D plot showing the effective potential U_{eff} as a color map, with the angle θ on the x-axis and the angle ϕ on the y-axis. The inset depicts the profile $U_{\text{eff}}(\theta)$ for $\phi = 0$, the introduced notations of ΔU_{eff} and θ_0 are presented. (b): Dependence of the initial angle θ_0 and the height of the potential barrier ΔU_{eff} on the external magnetic field H_{ext} .

Figure 2 illustrates two minima $U_{\text{eff}}(\theta, \phi)$ function corresponding to the two equilibrium states $\pm\theta_0$ and the barrier between them ΔU_{eff} . Numerical calculations are performed for material parameters typical for similar iron-garnets with compensation point [25, 26]: at the temperature of $T = 296$ K, $H_{\text{ext}} = 2527$ Oe, $K = 2660$ erg/cm³, $\chi = 9.4 \times 10^{-5}$, the Gilbert damping parameter $\alpha = 10^{-4}$, $m = 2.33$ emu/cm³, $(M_{Fe} - M_R)/(M_{Fe} + M_R) = 6 \cdot 10^{-3}$ (Appendix VII).

Thus, in RIG film in non-collinear phase there are two degenerate states with opposite sign of θ_0 angles. For realization of information writing and processing, these states can be treated as “0_w” (the potential well corresponding to $\theta_0 > 0$) and “1_w” ($\theta_0 < 0$), correspondingly.

III. BIT WRITING VIA OPTICAL MAGNETIZATION SWITCHING

Magnetization dynamics is determined by the motion equations for the angular variables θ and ϕ obtained from the Lagrangian function, see Appendix VII and Eq. (9) and (10) there. In contrast to previous researches (see [25, 26] for example) these equations are essentially non-linear as they describe dynamics in complex potential with two minima.

Fig. 3 presents the dynamics of the magnetization vector launched by femtosecond pulse of σ^+ circular polarization via inverse Faraday effect (IFE). The IFE is described by an optically generated effective magnetic field \mathbf{H}_{IFE} arisen from the interaction of the light's electric field with the medium and is proportional to the vector product of the electric field \mathbf{E} and its complex conjugate: $\mathbf{H}_{\text{IFE}} \propto [\mathbf{E} \times \mathbf{E}^*]$. The direction of \mathbf{H}_{IFE}

is parallel or antiparallel to the light k-vector depending on the helicity of the optical pulse. Due to a short duration of 0.05–0.2 ps, the impact of fs-pulse induced IFE is knock-like, so numerical solutions are obtained from the system of with initial conditions $\theta(0) = \theta_0$, $\phi(0) = 0$, $\frac{d\theta}{dt}|_{t=0} = \gamma^2(H_{\text{ext}} \cos(2\theta_0) - \frac{m}{\chi} \cos \theta_0) \tau H_{\text{IFE}}$, and $\frac{d\phi}{dt}|_{t=0} = 0$, where τ is the duration of a femtosecond pulse. Figure 3 (a) and (b) shows the temporal evolution of the polar and azimuthal angles, $\theta(t)$ and $\phi(t)$, respectively, for four distinct values of the effective field H_{IFE} , corresponding to different intensities of the circularly polarized excitation ($H_{\text{IFE}} = 1000$ Oe corresponds to $J = 4.4$ mJ/cm² fluence according to [26]).

In Fig. 3(c), the corresponding dynamical trajectories are visualized in a three-dimensional plot, where the z -axis represents the effective potential $U_{\text{eff}}(\theta, \phi)$. The numerically calculated trajectories $\theta(t)$ and $\phi(t)$, corresponding to the excitation by the circular polarized pulses with $\mathbf{H}_{\text{IFE}} = 500, 787, 790, 880$ Oe, are presented as the $U_{\text{eff}}(\theta(t), \phi(t))$.

As the energy of the optical pulse increases, the precession amplitude of the magnetization grows. At low energies ($\mathbf{H}_{\text{IFE}} = 500$ Oe), the system exhibits small-angle oscillations around the initial equilibrium. With the increase in pulse energy, the amplitude grows ($\mathbf{H}_{\text{IFE}} = 787$ Oe) and finally becomes large enough to overcome the potential barrier ($\mathbf{H}_{\text{IFE}} = 790$ Oe), resulting in magnetization switching: the system transitions from the initial equilibrium at $\theta_0 = 4.1$ deg to the opposite state at $-\theta_0$ (the trajectories with $H_{\text{IFE}} = 790, 880$ Oe in Fig. 3). This behavior reveals the existence of a threshold $H_{\text{IFE}}^{\sigma^+}$ required for switching (red solid line for $H_{\text{IFE}}^{\sigma^+}$ and blue for $H_{\text{IFE}}^{\sigma^-}$ in Fig. 4), above which the final equilibrium

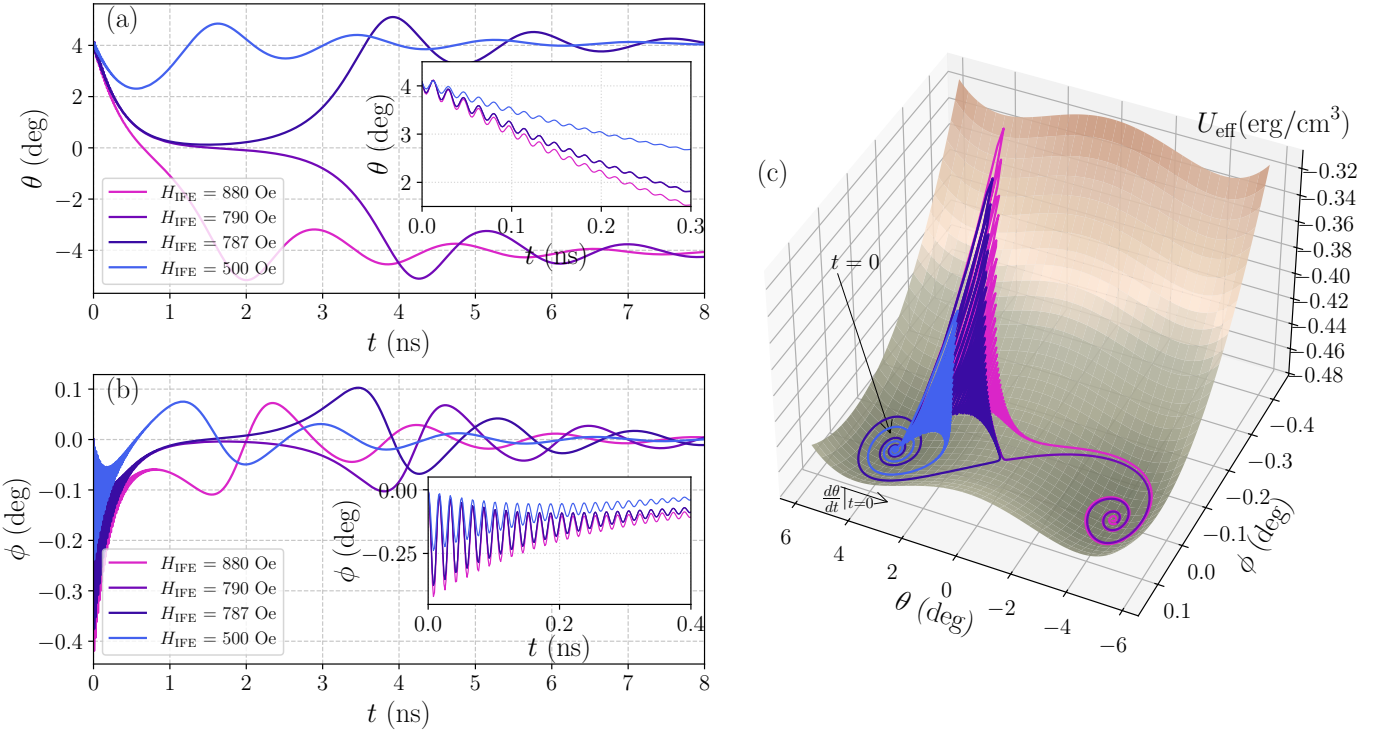


Figure 3: Dynamics of magnetization and effective potential landscape. Temporal evolution of $\theta(t)$ and $\phi(t)$ for different values of $H_{\text{IFE}} = 500, 787, 790, 880$ Oe acting on the system, (a) and (b), respectively. Insets display the same $\theta(t)$ and $\phi(t)$ but in a different time range. (c) 3D representation of the effective potential $U_{\text{eff}}(\theta, \phi)$ with superimposed dynamical trajectories $\phi(t)$ and $\theta(t)$. The parameters of numerical calculation: $T = 296$ K, $H_{\text{ext}} = 2527$ Oe, $K = 2660$ erg/cm³, $\chi = 9.4 \times 10^{-5}$, $\alpha = 10^{-4}$, $m = 2.33$ emu/cm³, $(M_{Fe} - M_R)/(M_{Fe} + M_R) = 6 \cdot 10^{-3}$

position is reversed. The corresponding pulse fluence estimated for the considered film is shown by the right axis of Fig. 4, the estimation was done using the data presented in Ref. [26].

Fig. 4 presents the dependence of the minimal effective field of the inverse Faraday effect required for optically-induced magnetization switching on the applied in-plane external magnetic field, H_{ext} . As the external field H_{ext} is varied, the corresponding point on the phase diagram shifts, leading to changes in both the shape of the effective potential and the initial equilibrium position θ_0 . This directly impacts the threshold IFE field required to induce switching.

An important feature observed in Fig. 4 is the difference between the switching threshold shown by the two curves: one corresponding to the σ_+ helicity where the initial angular velocity $\frac{d\theta}{dt}|_{t=0} < 0$ corresponds to the more favourable conditions (with representative trajectories illustrated in Fig. 3), and another for σ_- and $\frac{d\theta}{dt}|_{t=0} > 0$, where switching is notably less efficient compared to the positive case. The reason of such an asymmetry is Gilbert damping, which causes the system that is initially pushed away from the barrier to loose energy before its starts motion towards it. Thus, for $\theta_0 > 0$ and σ_+ helicity the system demonstrates a lower threshold for switching, than for σ_- . If the initial state is the opposite ($\theta_0 < 0$), the whole picture of dynamics is reversed,

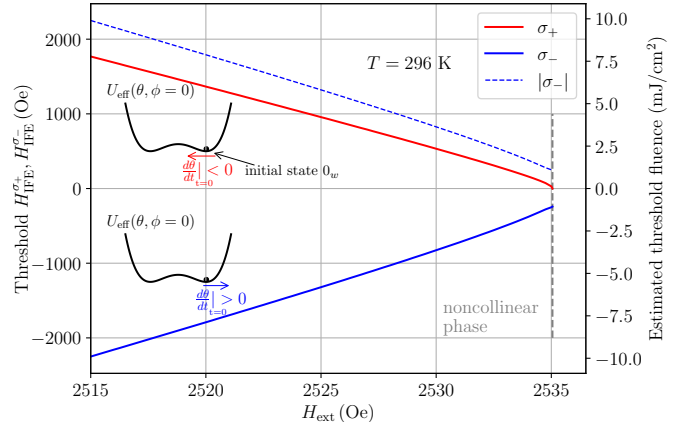


Figure 4: Dependence of the minimal effective inverse Faraday effect field H_{IFE} (left axis) and optical pump fluence (right axis) required for the magnetization switching on the applied in-plane external magnetic field H_{ext} . Two curves are shown: one corresponding to the case with positive initial angular velocity $\frac{d\theta}{dt}|_{t=0} < 0$ (right circular polarization σ_+), and another for $\frac{d\theta}{dt}|_{t=0} > 0$ (left circular polarization σ_-), where switching is less efficient.

and σ_- pulse provides lower threshold for switching. Absolute values of the IFE and fluences corresponding to

these lower and higher switching thresholds are denoted as $|H_{\text{IFE}}|^{min,max}$ and $J_{\text{min,max}}$.

Such a difference of the thresholds for σ_{\pm} femtosecond pulses is a key feature for deterministic information bit writing. If the energy of the femtosecond pulse J is enough to switch magnetization for a more favourable case $J > J_{\text{min}}$, and is less than the higher threshold value for the opposite helicity $J < J_{\text{max}}$, then the final state of the system is determined only by the pulse helicity. After σ_+ action the final state will be $-\theta_0$, which corresponds to writing “ 1_w ” magnetic bit, and after σ_- the final state will be θ_0 corresponding to “ 0_w ”, regardless of the initial state. Thus, optical information bit writing can be performed using the studied mechanism of optical switching of a ferrimagnet in non-collinear phase.

IV. OPTOMAGNONIC LOGIC

The ability to control the external magnetic field enables manipulation of the optically-induced magnetization switching process and the resulting magnetization state. For a fixed temperature, the external magnetic field H_{ext} and the corresponding equilibrium angle θ_0 (Fig. 2) set the initial state. The thresholds $H_{\text{IFE}}^{\sigma_+}$ and $H_{\text{IFE}}^{\sigma_-}$ (Fig. 4) quantify the minimum effective optical field needed to trigger a deterministic switching for the right- and left-circular excitation, respectively. By choosing the helicity of the optical pulse and tuning H_{ext} at the fixed temperature, it is possible to deterministically set the system into different logical states or to perform copying operations. This approach provides a pathway for implementing optical logic elements and memory operations in rare-earth iron garnet films.

Femtosecond laser pulses are used as the input of the proposed optomagnonic elements, while resulting magnetization state is the output. Let's assume that σ_+ helicity corresponds to “ 0_σ ” and σ_- corresponds to “ 1_σ ” and both pulses provide $|H_{\text{IFE}}| = 0.7$ kOe. For the two-input logic operations, femtosecond pulses encoded by σ_+ or σ_- helicity follow each other with a small delay Δt that exceeds the duration of the pulses (the duration of femtosecond pulses might vary in the range 0.1–100 ps) which is much smaller than the period of the low-frequency mode [26]. In this case, the action of these two pulses separated in time by Δt is independently summarized as

$$H_{\text{IFE}}^{(\text{sum})} = \pm H_{\text{IFE}}^1 \pm H_{\text{IFE}}^2, \quad (4)$$

with the sign before H_{IFE} is set by σ_{\pm} .

NOT gate. The simplest logical operation with one input is inversion (NOT gate). It may be performed using a single-pulse excitation of the ferrimagnet as discussed above. If the intensity of the pulse is just above the threshold, input “ 0_σ ” pulse excitation writes “ 1_w ” magnetic bit and vice versa. Table I shows realization of such a NOT gate. An external magnetic field is applied $H_{\text{ext}} = 2.53$ kOe, so that the module of equilibrium state angle is $\theta_0 = 3.23$ deg, potential barrier is

$\Delta U_{\text{eff}} = 7.5 \cdot 10^{-3}$ erg/cm³, lower switching threshold is $|H_{\text{IFE}}^{min}| = 533$ Oe ($J_{\text{min}} = 2.35$ mJ/cm²), and the higher is $|H_{\text{IFE}}^{max}| = 826$ Oe ($J_{\text{max}} = 3.63$ mJ/cm²). Such a configuration deterministically writes a magnetic bit of opposite value to the one that is encoded by the light helicity, as discussed above. If the initial state is “ 0_w ” then threshold values are $+533/-826$ Oe. Else at “ 1_w ” the threshold value changes the sign $-533/+826$ kOe.

Table I: Realization of NOT optomagnonic gate

Input	H_{IFE}	Initial state	Output
$0_\sigma (\sigma_+)$	+0.7 kOe	$0_w (+\theta_0)$	$1_w (-\theta_0)$
$0_\sigma (\sigma_+)$	+0.7 kOe	$1_w (-\theta_0)$	$1_w (-\theta_0)$
$1_\sigma (\sigma_-)$	-0.7 kOe	$0_w (+\theta_0)$	$0_w (+\theta_0)$
$1_\sigma (\sigma_-)$	-0.7 kOe	$1_w (-\theta_0)$	$0_w (+\theta_0)$

XNOR gate. XNOR has two inputs and should provide output “ 1_w ” in the case of the same inputs and “ 0_w ” in the case of the opposite inputs. It is realized by the application of the same external magnetic field $H_{\text{ext}} = 2.53$ kOe (all corresponding physical parameters are listed in NOT gate). This gate is initialized via one σ_- pulses with $H_{\text{IFE}} = -0.7$ kOe to put the system into “ 0_w ” magnetization state. Dynamics of the system under the action of consequent two input femtosecond pulses is shown in Fig. 5. The four panels demonstrate different scenarios of the double-pulse switching corresponding to XNOR truth table. Switching of the initial “ 0_w ” state occurs only under the action of the pulses of the same helicity, while the pulses of the opposite helicities compensate each other so that the system remains in “ 0_w ” state. Operation of XNOR gate is summarized in Table II.

NOR gate. NOR gate also has two inputs and the output is “ 0_w ” for the cases of at least one of the inputs is “ 1_σ ” (Table II). It is realized by the application of the external magnetic field $H_{\text{ext}} = 2.523$ kOe with corresponding parameters: $\theta_0 = 5$ deg, $\Delta U_{\text{eff}} = 4.2 \cdot 10^{-2}$ erg/cm³, $|H_{\text{IFE}}^{min}| = 1121$ Oe ($J_{\text{min}} = 4.93$ mJ/cm²), $|H_{\text{IFE}}^{max}| = 1511$ Oe ($J_{\text{max}} = 6.65$ mJ/cm²). This gate is initialized via two consequent σ_- pulses with $H_{\text{IFE}} = -0.7$ kOe each putting the system to “ 0_w ” magnetization state (in this case threshold values are $+1121/-1511$ Oe). Switching to “ 1_w ” from the initial “ 0_w ” magnetization state requires two σ_+ pulses, as illustrated in Table II, while all other combinations provide “ 0_w ” output.

NAND gate. NAND gate performs negation of the conjunction operation, providing the output “ 0_w ” only for the case of two “ 1_σ ” inputs. It is realized by the application of the same external magnetic field $H_{\text{ext}} = 2.523$ kOe, as for NOR gate. However, initialization is performed via two consequent σ_+ pulses with $H_{\text{IFE}} = +0.7$ kOe each putting the system to “ 1_w ” initial magnetization state (in this case threshold values are $-1121/+1511$ Oe). Output “ 0_w ” thus requires magnetization switching, which is realized only for the case of

two σ_- pulses, see Table II, while all other combinations provide “ 1_w ” output.

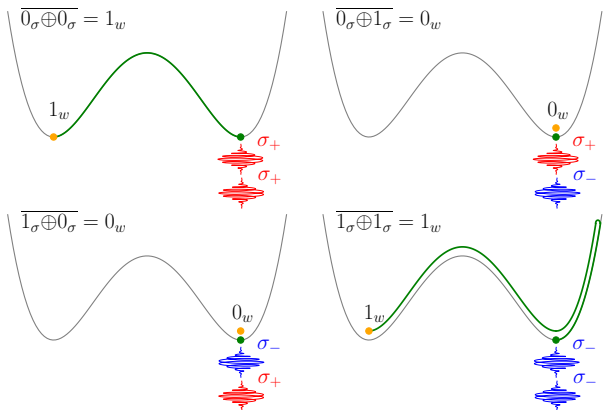


Figure 5: The realization of XNOR gate with $H_{\text{ext}} = 2.53$ kOe, and the input bits “ 0_σ ” and “ 1_σ ”, encoded by $H_{\text{IFE}} = \pm 0.7$ kOe, respectively. The form of potential $U_{\text{eff}}(\phi = 0, \theta)$ is illustrated by gray solid lines, the initial state corresponds to “ 0_w ” (green dot), the output bits “ 0_w ” and “ 1_w ” are depicted by orange dots.

Table II: Realization of XNOR, NOR and NAND optomagnetic gates

XNOR gate ($H_{\text{ext}} = 2.53$ kOe)			
Input 1	Input 2	$H_{\text{IFE}}^{(\text{sum})}$	Output
0_σ (σ_+)	0_σ (σ_+)	+1.4 kOe	1_w ($-\theta_0$)
0_σ (σ_+)	1_σ (σ_-)	0 kOe	0_w ($+\theta_0$)
1_σ (σ_-)	0_σ (σ_+)	0 kOe	0_w ($+\theta_0$)
1_σ (σ_-)	1_σ (σ_-)	-1.4 kOe	1_w ($-\theta_0$)
NOR gate ($H_{\text{ext}} = 2.523$ kOe)			
Input 1	Input 2	$H_{\text{IFE}}^{(\text{sum})}$	Output
0_σ (σ_+)	0_σ (σ_+)	+1.4 kOe	1_w ($-\theta_0$)
0_σ (σ_+)	1_σ (σ_-)	0 kOe	0_w ($+\theta_0$)
1_σ (σ_-)	0_σ (σ_+)	0 kOe	0_w ($+\theta_0$)
1_σ (σ_-)	1_σ (σ_-)	-1.4 kOe	0_w ($+\theta_0$)
NAND gate ($H_{\text{ext}} = 2.523$ kOe)			
Input 1	Input 2	$H_{\text{IFE}}^{(\text{sum})}$	Output
0_σ (σ_+)	0_σ (σ_+)	+1.4 kOe	1_w ($-\theta_0$)
0_σ (σ_+)	1_σ (σ_-)	0 kOe	1_w ($-\theta_0$)
1_σ (σ_-)	0_σ (σ_+)	0 kOe	1_w ($-\theta_0$)
1_σ (σ_-)	1_σ (σ_-)	-1.4 kOe	0_w ($+\theta_0$)

Other gates. The family of ferrimagnet-based optomagnetic elements can be extended to multi-input gates in a similar way as discussed above. In this case, the external magnetic field should be adjusted so that only one of the multi-input combinations provides sum IFE suitable for magnetization switching. Also, the reversal of

operations (NOR, NAND, XOR) can be performed based on the elements described above with an additional post-processing pulse with IFE above the switching threshold.

Stability. At finite temperature, there is a finite probability for the magnetization to flip and reverse its direction. The mean time between two flips is called the Néel relaxation time τ_N and is given by the Néel-Arrhenius equation [39–41] $\tau_N = \tau_0 \exp[\Delta U_{\text{eff}} V / (kT)]$, where V is the volume of remagnetized area and $1/\tau_0$ is an attempt frequency [42], which describes the probability of magnetization reversal and has the typical values of 10^9 Hz [40, 41]. For the configuration used above and magnetic bit size $10 \times 10 \times 1.8 \mu\text{m}$ ($V = 1.8 \cdot 10^{-10} \text{ cm}^3$), $\Delta U_{\text{eff}} = 0.0075 \text{ erg/cm}^3$ and $T = 296$ K. The relation $\frac{\Delta U_{\text{eff}} V}{kT} = 33$ holds, and, therefore, $\tau_N \approx 3$ days, which is sufficiently large for logic operations. Stable smaller bits are available if higher potential barriers are used.

Reading. As the result of logical operation is written as the magnetization state of a ferrimagnet, it can be read by either traditional means using electromagnetic coils, or using ultrafast magneto-optical reading via linearly-polarized low-energy optical pulses. In the latter case, the sign of the probe Faraday rotation provides a direct measure of written magnetic bit, closing the logic loop without requiring electrical contacts with unavoidable heating.

V. CONCLUSION

We have theoretically and numerically investigated spin dynamics and optically-induced magnetization switching in a bistable rare-earth iron garnet with magnetization compensation point. Magnetization switching is launched via the optomagnetic effect, inverse Faraday effect, namely. It exhibits a threshold of effective field amplitude under which the switching is observed. This threshold depends on the applied external magnetic field and the helicity of the incident optical pulse. This makes it possible to deterministically put the system into the desired magnetization state, and to write a magnetic bit. The dependence of the switching threshold on the optical pulse fluence and helicity opens new possibilities for construction of the optomagnetic logic elements. We have elaborated the design of all basic logical elements (NOT, AND, OR, XOR and their negations) based on the discussed optomagnetic switching effect. The dependence of the switching threshold on the applied external magnetic field provides a unique feature of reconfigurability of optomagnetic logic elements, i.e. a possibility to change on-the-fly the type of the performed logical operation. These results highlight the potential of rare-earth iron garnets as a material platform for fast, energy-efficient and reconfigurable optomagnetic logics, and provoke future experimental implementations of optomagnetic computing devices.

VI. ACKNOWLEDGMENTS

This work was financially supported by Russian Science Foundation (project №23-62-10024).

VII. APPENDIX

The Lagrangian formalism is employed to describe the dynamics of the sublattice magnetization vectors and derive the equations of motion for the antiferromagnetic vector \mathbf{L} , parameterized by spherical angles θ and ϕ as $\mathbf{L} = L(\cos \theta \cos \phi, \cos \theta \sin \phi, \sin \theta)$. The two-sublattice system is characterized by the rare-earth (\mathbf{M}_R) and iron (\mathbf{M}_{Fe}) magnetization vectors, with magnitudes M_R and M_{Fe} , and spherical angles θ_R, ϕ_R and θ_{Fe}, ϕ_{Fe} , respectively ($\mathbf{M}_i = M_i(\cos \theta_i \cos \phi_i, \cos \theta_i \sin \phi_i, \sin \theta_i)$ with $i = R, Fe$).

The angles of antiferromagnetic vector and two sublattices are related by

$$\theta_{Fe} = \theta + \varepsilon, \quad \theta_R = -\theta + \varepsilon, \quad (5)$$

$$\phi_{Fe} = \phi + \beta, \quad \phi_{Fe} = \pi + \phi - \beta, \quad (6)$$

where the parameters $\varepsilon \ll 1$ and $\beta \ll 1$ characterize the noncollinearity of the magnetization vectors of the sublattices [25]. The Lagrangian of the system is given by [25, 28, 37, 38] and rewritten using $\theta, \varepsilon, \phi, \beta$:

$$\mathcal{L} = -\frac{m}{\gamma} \sin \theta \dot{\phi} - \frac{M}{\gamma} (\epsilon \dot{\phi} - \beta \dot{\theta}) \cos \theta - \Phi, \quad (7)$$

where $\gamma = \gamma_{Fe} = \gamma_R$ is the gyromagnetic ratios assumed equal for both sublattices, Φ is the potential energy [25, 43], $M = M_{Fe} + M_R$ is the sum of the sublattice magnetizations, $m = M_{Fe} - M_R$ is the difference between the sublattice magnetizations. The effect of an external magnetic field H_{ext} is also considered in potential energy, under the assumption that the applied field is much weaker than the exchange field.

The equilibrium states of the two-sublattice system are found as the minimum of the effective potential energy obtained using the known relationship between the Lagrange and the Hamiltonian functions for the stationary case $\dot{\theta} = 0$ and $\dot{\phi} = 0$:

$$U_{eff} = -\frac{\chi}{2} H_{ext}^2 (\sin^2 \theta \cos^2 \phi + \sin^2 \phi) - m H_{ext} \cos \theta \cos \phi - K \sin^2 \theta, \quad (8)$$

Eq. 8 shows that antiferromagnetic vector \mathbf{L} in the equilibrium state characterized by θ_0 and ϕ_0 angles. In the $H_{ext} - T$ phase diagram $\theta_0(H_{ext}, T)$ of a ferrimagnet two main phases are possible: collinear and non-collinear ones [25], that are presented in Fig. 6.

In order to derive the Euler–Lagrange equations for the angles θ and ϕ describing the antiferromagnetic vector \mathbf{L}

[25], we employ the Lagrangian and Rayleigh dissipation

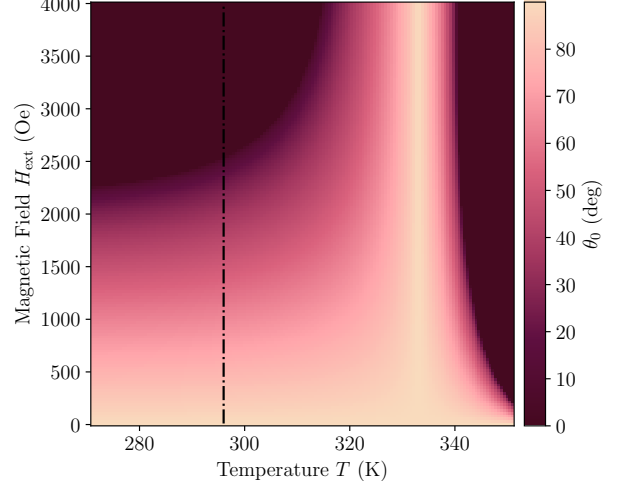


Figure 6: $\theta_0(H_{ext}, T)$ phase diagram using the parameters from Section II.

functions[25]. This approach allows us to obtain a system of second-order differential equations governing the dynamics of these two variables

$$-\frac{M^2 \ddot{\theta}}{\delta \gamma^2} + \frac{M^2 H_{ext}}{\delta \gamma} \dot{\phi} \cos \phi - \frac{M^2}{\delta} \left(\frac{\dot{\phi}^2}{\gamma^2} \sin \theta \cos \theta - H_{ext}^2 \sin \theta \cos \theta \cos^2 \phi - \frac{\dot{\phi}}{\gamma} H_{ext} \cos \phi \cos 2\theta \right) - \dot{\phi} \frac{m}{\gamma} \cos \theta - m H_{ext} \sin \theta \cos \phi + K \sin 2\theta = \frac{\alpha M}{\gamma} \dot{\theta} \quad (9)$$

$$\frac{M^2}{\delta \gamma} \left(-\frac{\dot{\phi}}{\gamma} \dot{\theta} \sin 2\theta + H_{ext} \dot{\phi} \cos 2\theta \cos \phi - H_{ext} \dot{\phi} \sin \theta \cos \theta \sin \phi + \frac{\ddot{\phi}}{\gamma} \cos^2 \theta \right) - \frac{m}{\gamma} \dot{\theta} \cos \theta + \frac{M^2}{\delta} \left(\frac{\dot{\phi}}{\gamma} H_{ext} \sin \theta \cos \theta \sin \phi + \frac{\dot{\theta}}{\gamma} H_{ext} \cos \phi \right) + H_{ext}^2 \sin^2 \theta \cos \phi \sin \phi - H_{ext}^2 \cos \phi \sin \phi + m H_{ext} \cos \theta \sin \phi = -\frac{\alpha M}{\gamma} \dot{\phi} \cos^2 \theta \quad (10)$$

where α is the Hilbert damping parameter, $\delta = 2\Lambda M_{Fe} M_R$ is the difference between the sublattice magnetizations, $\Lambda > 0$ is the intersublattice exchange constant and the “+” sign of the second term represents the antiferromagnetic character of the exchange interaction between the sublattices. These equations describe the dynamics of the system in the presence of damping and external forces, and are valid within the quasi-antiferromagnetic approximation.

[1] S. Wang, C. Wei, Y. Feng, H. Cao, W. Li, Y. Cao, B.-O. Guan, A. Tsukamoto, A. Kirilyuk, A. V. Kimel, *et al.*, Dual-shot dynamics and ultimate frequency of all-optical magnetic recording on gdfeco, *Light: Science & Applications* **10**, 8 (2021).

[2] A. Kirilyuk, A. V. Kimel, and T. Rasing, Ultrafast optical manipulation of magnetic order, *Reviews of Modern Physics* **82**, 2731 (2010).

[3] M. Hennecke, D. Schick, T. P. Sidiropoulos, J.-X. Lin, Z. Guo, G. Malinowski, M. Mattern, L. Ehrentraut, M. Schmidbauer, M. Schnuerer, *et al.*, Transient domain boundary drives ultrafast magnetisation reversal, *Nature Communications* **16**, 8233 (2025).

[4] A. Stupakiewicz, K. Szerenos, D. Afanasiev, A. Kirilyuk, and A. Kimel, Ultrafast nonthermal photo-magnetic recording in a transparent medium, *Nature* **542**, 71 (2017).

[5] A. Stupakiewicz, K. Szerenos, M. Davydova, K. Zvezdin, A. Zvezdin, A. Kirilyuk, and A. Kimel, Selection rules for all-optical magnetic recording in iron garnet, *Nature communications* **10**, 612 (2019).

[6] P. Li, T. J. Kools, H. Pezeshki, J. M. Joosten, J. Li, J. Igarashi, J. Hohlfeld, R. Lavrijsen, S. Mangin, G. Malinowski, *et al.*, Picosecond all-optical switching of co/gd-based synthetic ferrimagnets, *Physical Review B* **111**, 064421 (2025).

[7] J. Li, Q. Guo, T. Lin, Q. Zhang, H. Bai, S. Cheng, X. Zhan, L. Gu, and T. Zhu, Field-free magnetization switching through large out-of-plane spin-orbit torque in the ferromagnetic copt single layers, *Applied Physics Letters* **124** (2024).

[8] J. Hintermayr and B. Koopmans, Explaining all-optical switching in ferrimagnets with heavy rare-earth elements by varying the spin-flip scattering probability of gd in coxgd100- x alloys and co/gd bilayers, *Journal of Magnetism and Magnetic Materials* **603**, 172260 (2024).

[9] G.-Q. Li, X.-Y. Zheng, J.-L. Wang, X.-Y. Lu, J. Wu, J.-W. Cai, H. Meng, B. Liu, T. A. Ostler, and Y.-B. Xu, Timescales and contribution of heating and helicity effect in helicity-dependent all-optical switching, *Rare Metals* **42**, 234 (2023).

[10] K. T. Yamada, C. S. Davies, F. Ando, T. Li, T. Ono, T. Rasing, A. V. Kimel, and A. Kirilyuk, Magnetization reversal of a ferromagnetic pt/co/pt film by helicity dependent absorption of visible to near-infrared laser pulses, *Physical Review B* **111**, L020406 (2025).

[11] P. K. Pal, A. K. Mondal, and A. Barman, Using magnons as a quantum technology platform: a perspective, *Journal of Physics: Condensed Matter* **36**, 441502 (2024).

[12] P. Pirro, V. I. Vasyuchka, A. A. Serga, and B. Hillebrands, Advances in coherent magnonics, *Nature Reviews Materials* **6**, 1114 (2021).

[13] K. Wang, Y.-P. Gao, R. Jiao, and C. Wang, Recent progress on optomagnetic coupling and optical manipulation based on cavity-optomagnonics, *Frontiers of Physics* **17**, 42201 (2022).

[14] S. Mangin, M. Gottwald, C. Lambert, D. Steil, V. Uhlíř, L. Pang, M. Hehn, S. Alebrand, M. Cinchetti, G. Malinowski, *et al.*, Engineered materials for all-optical helicity-dependent magnetic switching, *Nature materials* **13**, 286 (2014).

[15] C. Banerjee, N. Teichert, K. Siewierska, Z. Gercsi, G. Atcheson, P. Stamenov, K. Rode, J. Coey, and J. Besbas, Single pulse all-optical toggle switching of magnetization without gadolinium in the ferrimagnet mn2ruxga, *Nature communications* **11**, 4444 (2020).

[16] W.-Y. Choi, J.-H. Ha, M.-S. Jung, S. B. Kim, H. C. Koo, O. Lee, B.-C. Min, H. Jang, A. Shahee, J.-W. Kim, *et al.*, Magnetization switching driven by magnonic spin dissipation, *Nature Communications* **16**, 5859 (2025).

[17] T. Ostler, J. Barker, R. Evans, R. Chantrell, U. Atxitia, O. Chubykalo-Fesenko, S. El Moussaoui, L. Le Guyader, E. Mengotti, L. Heyderman, *et al.*, Ultrafast heating as a sufficient stimulus for magnetization reversal in a ferrimagnet, *Nature communications* **3**, 666 (2012).

[18] C. D. Stanciu, F. Hansteen, A. V. Kimel, A. Kirilyuk, A. Tsukamoto, A. Itoh, and T. Rasing, All-optical magnetic recording with circularly polarized light, *Physical review letters* **99**, 047601 (2007).

[19] K. Vahaplar, A. Kalashnikova, A. Kimel, D. Hinzke, U. Nowak, R. Chantrell, A. Tsukamoto, A. Itoh, A. Kirilyuk, and T. Rasing, Ultrafast path for optical magnetization reversal via a strongly nonequilibrium state, *Physical review letters* **103**, 117201 (2009).

[20] T. Zalewski, A. Maziewski, A. Kimel, and A. Stupakiewicz, Ultrafast all-optical toggle writing of magnetic bits without relying on heat, *Nature Communications* **15**, 4451 (2024).

[21] L. Pitaevskii, Electric forces in a transparent dispersive medium, *Sov. Phys. JETP* **12**, 1008 (1961).

[22] J. Van der Ziel, P. S. Pershan, and L. Malmstrom, Optically-induced magnetization resulting from the inverse faraday effect, *Physical review letters* **15**, 190 (1965).

[23] K.-K. Wu, H.-M. Lee, J. Xu, P.-Y. Yang, C. Chien, S.-Y. Huang, and D. Qu, Magnon spin current from a non-collinear magnetic phase in a compensated rare earth ferrimagnet, *Applied Physics Letters* **124** (2024).

[24] M. Davydova, K. Zvezdin, J. Becker, A. Kimel, and A. Zvezdin, H-t phase diagram of rare-earth-transition-metal alloys in the vicinity of the compensation point, *Physical Review B* **100**, 064409 (2019).

[25] D. Krichevsky, N. Gusev, D. Ignatyeva, A. Prisyazhnyuk, E. Y. Semuk, S. Polulyakh, V. Berzhansky, A. Zvezdin, and V. Belotelov, Unconventional spin dynamics in the noncollinear phase of a ferrimagnet, *Physical Review B* **108**, 174442 (2023).

[26] D. Ignatyeva, N. Gusev, I. Prilepsky, A. Prisyazhnyuk, D. Krichevsky, S. Polulyakh, V. Berzhansky, A. Zvezdin, and V. Belotelov, High-amplitude ferromagnetic soft mode at the spin-reorientation transition in an iron garnet film excited by ultrashort laser pulses, *Physical Review B* **111**, 224424 (2025).

[27] D. Ignatyeva, N. Gusev, A. Zvezdin, and V. Belotelov, Spin-reorientation and phase diagram for a ferrimagnet with compensation point in inclined magnetic field, *Journal of Magnetism and Magnetic Materials* **623**, 172968 (2025).

[28] T. G. Blank, K. Grishunin, E. Mashkovich, M. Logunov, A. Zvezdin, and A. Kimel, Thz-scale field-induced spin dynamics in ferrimagnetic iron garnets, *Physical Review Letters* **127**, 037203 (2021).

- [29] M. Deb, P. Molho, B. Barbara, and J.-Y. Bigot, Controlling laser-induced magnetization reversal dynamics in a rare-earth iron garnet across the magnetization compensation point, *Physical Review B* **97**, 134419 (2018).
- [30] A. Stupakiewicz and T. Satoh, Ultrafast optomagnonics in ferrimagnetic multi-sublattice garnets, *Journal of the Physical Society of Japan* **90**, 081008 (2021).
- [31] B. Ivanov, Ultrafast spin dynamics and spintronics for ferrimagnets close to the spin compensation point, *Low Temperature Physics* **45**, 935 (2019).
- [32] A. C. Kaczmarek, E. R. Rosenberg, Y. Song, K. Ye, G. A. Winter, A. N. Penn, R. Gomez-Bombarelli, G. S. Beach, and C. A. Ross, Atomic order of rare earth ions in a complex oxide: a path to magnetotaxial anisotropy, *Nature Communications* **15**, 5083 (2024).
- [33] S. Geller, J. Remeika, R. Sherwood, H. Williams, and G. Espinosa, Magnetic study of the heavier rare-earth iron garnets, *Physical Review* **137**, A1034 (1965).
- [34] C. Dubs and O. Surzhenko, Magnetically compensated nanometer-thin ga-substituted yttrium iron garnet (ga: Yig) films with robust perpendicular magnetic anisotropy, *arXiv preprint arXiv:2504.03377* (2025).
- [35] S. Schlauderer, C. Lange, S. Baierl, T. Ebnet, C. P. Schmid, D. Valovcin, A. Zvezdin, A. Kimel, R. Mikhaylovskiy, and R. Huber, Temporal and spectral fingerprints of ultrafast all-coherent spin switching, *Nature* **569**, 383 (2019).
- [36] S. Baierl, M. Hohenleutner, T. Kampfrath, A. Zvezdin, A. Kimel, R. Huber, and R. Mikhaylovskiy, Nonlinear spin control by terahertz-driven anisotropy fields, *Nature Photonics* **10**, 715 (2016).
- [37] M. Davydova, K. Zvezdin, A. Kimel, and A. Zvezdin, Ultrafast spin dynamics in ferrimagnets with compensation point, *Journal of Physics: Condensed Matter* **32**, 01LT01 (2019).
- [38] A. Zvezdin, Dynamics of domain walls in weak ferromagnets, *ZhETF Pisma Redaktsiiu* **29**, 605 (1979).
- [39] L. Néel, Théorie du trainage magnétique des ferromagnétiques en grains fins avec application aux terres cuites, in *Annales de géophysique*, Vol. 5 (1949) pp. 99–136.
- [40] Z. Li and S. Zhang, Thermally assisted magnetization reversal in the presence of a spin-transfer torque, *Physical Review B* **69**, 134416 (2004).
- [41] S. Bance, J. Fischbacher, A. Kovacs, H. Oezelt, F. Reichel, and T. Schrefl, Thermal activation in permanent magnets, *Jom* **67**, 1350 (2015).
- [42] G. Fiedler, J. Fidler, J. Lee, T. Schrefl, R. Stamps, H. Braun, and D. Suess, Direct calculation of the attempt frequency of magnetic structures using the finite element method, *Journal of Applied Physics* **111** (2012).
- [43] K. P. Belov, A. K. Zvezdin, A. M. Kadomtseva, and R. Z. Levitin, Spin-reorientation transitions in rare-earth magnets, *Soviet Physics Uspekhi* **19**, 574 (1976).